Aggregate Open Access WILEY

Chiral dual-core AIEgens based-on through-space coupling for high-performance organic light-emitting diodes with little efficiency roll-off

Lifen Chen, Mingjia Deng, Shao-Yun Yin, Yu Fu, Yingxiao Mu,* Jia-Xiong Chen, Lingyun Cui,* Shaomin Ji, Yanping Huo* and Hao-Li Zhang*

L. Chen, M. Deng, Y. Fu, Dr. Y. Mu, Dr. J.-X. Chen, Prof. S. Ji, Prof. Y. Huo, Prof. H.-L. Zhang
School of Chemical Engineering and Light Industry, Guangdong University of Technology, Guangzhou, 510006, P.R. China
E-mail: yxmu@gdut.edu.cn; yphuo@gdut.edu.cn

Dr. L. Cui
Beijing City University
Beijing, 100083, P.R. China
E-mail: cly@iccas.ac.cn

Dr. S.-Y. Yin, Prof. Y. Huo
Analysis and Test Center
Guangdong University of Technology
Guangzhou, 510006, P.R. China

Prof. H.-L. Zhang
State Key Laboratory of Applied Organic Chemistry (SKLAOC),
College of Chemistry and Chemical Engineering
Lanzhou University
Lanzhou, 730000, P.R. China
E-mail: haoli.zhang@lzu.edu.cn

Keywords: aggregation-induced emission, thermally activated delayed fluorescence, through-space coupling, circularly polarized luminescence, organic light-emitting diodes

In this work, we demonstrate a chiral dual-core strategy for the design of high-performance organic circularly polarized aggregation-induced emission luminogens (AIEgens), which features of connecting two thermally activated delayed fluorescence (TADF) luminophore with chiral linkage that allows efficient through-space coupling (TSC) to occur. Using this strategy, a pair of dual-core enantiomers, R/S-DNKP, were designed and synthesized by linking two benzophenone derivatives with a 1,1'-bi-2-naphthol unit. Compared to the mono-core counterpart NKP, the dual-core emitters exhibited a much higher photoluminescence quantum yields of 94%. Moreover, benefited from their chiral helical folding configurations, the R/S-

DNKP enantiomers exhibited a high luminescence dissymmetry factor ($|g_{lum}|$) value up to 1.3×10^{-3} in film states. Notably, the electroluminescence devices based on the R/S-DNKP enantiomers achieved external quantum efficiency values of 21.5% and 19.7% with little roll-off. It is believed that this molecular design strategy will pave new routes for the development of high-performance chiral emitters for future organic photonic devices.

1. Introduction

Organic light-emitting diodes (OLEDs) are becoming one of the important applications for solid-state display and lighting due to the superior characteristics such as flexibility, large area, high-quality color and lightweight.[1] To achieve the commercial application of OLEDs, large external quantum efficiency (EQE) and small electroluminescence (EL) efficiency roll-off for devices at high luminance values are required.[2] However, the charge carriers in the emissive layer of OLEDs undergo unbalanced recombination with the increase of voltage, which often leads to low EQE and severe efficiency roll-off.[3] Currently, thermally activated delayed fluorescence (TADF) materials with aggregation-induced emission (AIE) characteristics have been considered as one of the most promising organic EL materials.[4] It is known that TADF materials with suitable twisted geometry of the donor-acceptor (D-A) structure could achieve a small singlet-triplet state energy gap (ΔE_{ST}) to facilitate the RISC process.[5] And the distorted conformation favours the suppression of exciton annihilation in the aggregated state.[6] Therefore, AIE-TADF materials owned both high photoluminescence quantum yield (PLQY) and accelerated RISC process are expected to work as high-performance emitters in OLEDs with small roll-off. Meanwhile, it has been reported that integration of dual TADF luminogenic cores in one emitter molecule and increased the molecular stiffness may suppress the non-radiative transition process to improve PLQY.[7] In such molecular design, efficient electronic coupling between the two cores are essential to tailor the luminescence property of the whole

systems.[8] So far most molecular designs were based on directly connecting the two cores by σ bonds, which enable through-bond coupling,[9] such as the examples illustrated in Figure 1.

Circularly polarized luminescence (CPL) which relies on emitters with chiral structures has attracted wide attention for the potential applications in three-dimensional display, optical data storage and quantum computing.[10] Design of pure organic CPL emitters is still challenging at the moment. The majority of organic CPL emitters exhibits luminescence dissymmetry factor ($|g_{lum}|$) values below 10^{-3} in solid state.[11] In addition to through-bond coupling strategy described above, designing the molecular conformation to allow through-space coupling (TSC) to occur could also be an efficient method to control the spatial delocalization of π electrons, which caused by non-covalent excitonic coupling in closely aspectant overlapped aromatic rings.[12] Recent researches have demonstrated that TSC could have important effects on the absorption, intramolecular charge transfer and bipolar charge transport properties of luminescent materials.[13] Several luminescent materials utilizing TSC have successfully used in OLEDs, either as light-emitting or hole/electron-transporting layers.[14] Though shown promising applications, high performance small molecular emitters containing dual TADF units based-on TSC has rarely been explored to date. Utilizing TSC in molecular design offered more freedom in the selection of the connecting units between the two luminogenic cores and supplied more efficient orbitals interaction and overlap, as the conjugation length of the linkage unit is no longer important while the conformation and the spatial arrangement become crucial. We herein point out that such design freedom also provides an opportunity to incorporate large chiral unit as linkage unit. Incorporating chiral unit into fluorescent materials is highly desirable for the study of CPL emitter. Most circularly polarized TADF materials reported so far have chiral units, such as 1,1'-bi-2-naphthol (BINOL),[15] attached as side groups. However, taking advantage of the design of freedom of utilizing TSC, one can conveniently introduce a large aromatic chiral unit in the central position for enhanced CPL properties.

To verify the above proposition, we demonstrate herein a chiral dual-core strategy for the design of high-performance CPL emitters that also facilitating high EQE and little efficiency roll-off in OLEDs. As a proof of concept, a pair of enantiomers, namely R/S-DNKP, are constructed, which consists of dual benzophenone emitting cores linked by a BINOL unit in the central position (Figure 1). In this design, each benzophenone is linked with a phenoxazine unit to give localized D-A structures, in which benzophenone acts as acceptor and the phenoxazine acts as donor. Importantly, a spatial coupling effect caused by the chiral helical folding configuration is enabled between the binaphthol and the adjacent benzophenone units, giving strong intramolecular TSC effects. The enantiomers present mirror-image circular dichroism (CD) and excellent CPL activities with the luminescence dissymmetry factors (g_{lum}) values up to $+1.1\times10^{-3}$ and -1.3×10^{-3} in film states, respectively. Moreover, the dual-core molecules R/S-DNKP exhibit remarkably enhanced absorption coefficients, thermal stability, PLQY and high-efficiency RISC, as compared with the single-core counterpart NKP. Consequently, the OLED devices based on the R/S-DNKP exhibit a high EQE_{max} of 21.5%, and an extremely small efficiency roll-off of 2.5% at high luminance of 5000 cd m^{-2}. All the results indicate that this chiral dual-core strategy is efficient in the rational design of high-performance chiral emitters.

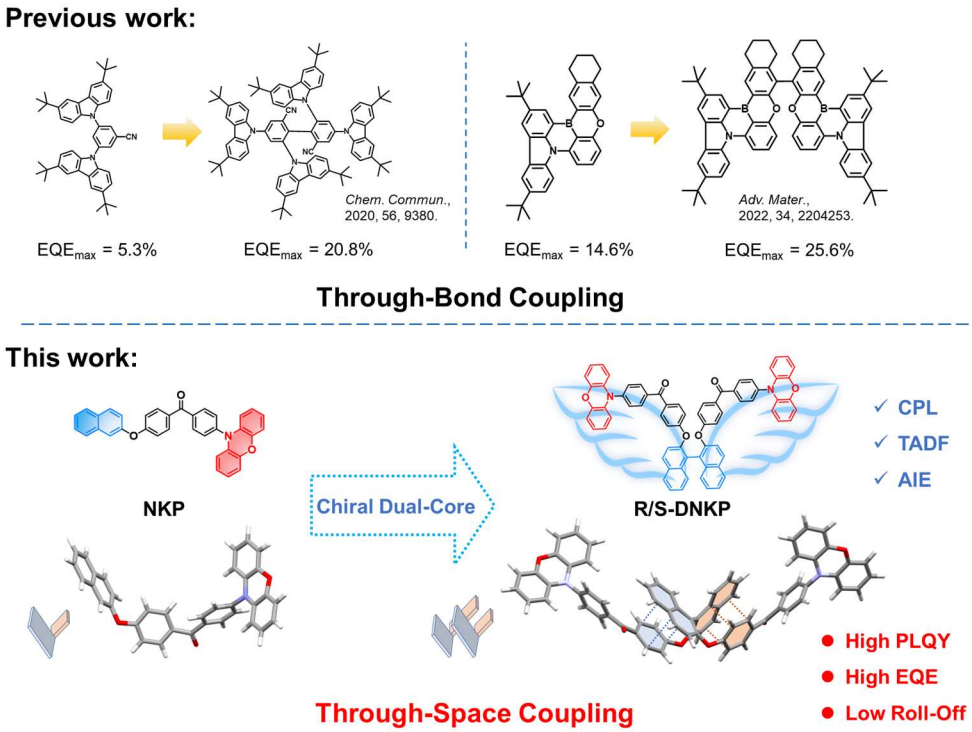

Figure 1. Illustration of reported dual-core emitter and this work.

2. Results and discussion

2.1. Synthesis and Characterization

The dual-core enantiomers R/S-DNKP and mono-core NKP were designed and synthesized with high yields and the synthetic routes were shown in Scheme S1. The emitters R/S-DNKP were conveniently prepared by nucleophilic substitution of two bis(4-fluorophenyl)-methanone with R/S-1,1'-Bi-2-naphthol, respectively, followed a subsequent substitution reaction with phenoxazines. We selected 4,4'-Bis(N-carbazolyl)-1,1'-biphenyl (CBP) as the host material to prepare the doped film. In addition, NKP was synthesized by similarly procedures with naphthol as substituent group. All new compounds were thoroughly characterized by ^{1}H NMR, ^{13}C NMR and high-resolution mass spectrometry as shown in the supporting information (Figures S1-S12).

2.2. Photophysical Properties

The UV-visible absorption and photoluminescence (PL) spectra of of R-DNKP and NKP in tetrahydrofuran (THF) solution with the concentration of 10^{-5} M were shown in the Figure 2a. It exhibited strong absorption peak with π-π* transitions around 300 nm. Besides, the broad absorption band from 380 to 420 nm was assigned to the n-π* transitions which rooting from the phenoxazine to benzophenone moiety. The attribution of the UV transitions and bands could be supported by theoretical calculations in Figure S13. The R-DNKP showed the maximum absorption coefficient of 4.82×10^4 M^{-1} cm^{-1} compared with 2.35×10^4 M^{-1} cm^{-1} for NKP, indicating intensified light absorption and the extension of conjugation caused by the linkage between two coupled core moieties. And the PL spectra in different dilute solutions exhibited obvious solvatochromism effect, the structureless bands can be verified that the charge transfer feature in their excited states. Furthermore, the extension of coupling caused by dual emitting cores led to red-shifts of emission peaks for the R-DNKP compared to NKP. As shown in Figure S14, with increasing the solvent polarities gradually from n-hexane (Hex), toluene (Tol) and THF, the emission peak position of R-DNKP was red-shifted from 512 nm to 620 nm, while that of NKP was from 504 nm to 615 nm. The corresponding PL spectra of R-DNKP and NKP with different THF/water ratios were investigated to validate the AIE property in Figures 2c-d and S15. Taking the spectra of R-DNKP as example, R-DNKP showed an orange-red fluorescence with maximum emission at 620 nm in pure THF solution. As the water fraction increased from 0% to 70%, the emission was extremely weak and the spectra redshifted to about 650 nm. When the water fraction exceeds 70%, the PL intensity increases rapidly with blue-shifted profile. After formation of the aggregates, the intramolecular dipole-dipole interaction weakens in comparison to the polar solvent interaction, demonstrating the prominent AIE property of enantiomers.[19]

To deepen the understanding of the luminescent property in solid state, emission properties at room temperature and 77 K were studied to obtain the ΔE_{ST} value of the neat and doped film (Figure S16). The calculated ΔE_{ST} values for neat films of R-DNKP and NKP were 0.09 and 0.10 eV, respectively. By contrast, the measured ΔE_{ST} values of both materials were obtained to be 0.07 and 0.08 eV, respectively, in the co-doped film (20 wt % doped in CBP). Thus, such a small ΔE_{ST} can support the fact that both materials might exhibit TADF properties with effective RISC process from T_1 to S_1. The absolute PLQY measured using an integrating sphere for R-DNKP in the neat film and doped film were 75% and 94%, respectively, and the corresponding value for NKP were 68% and 88%, respectively. (Table 1)

The transient PL decay characteristics were then measured in the neat and doped film under vacuum to confirm their TADF properties. As shown in Figures 2b and S17, the ratio of the delayed component in the transient PL spectra were gradually increased from 100 to 300 K, indicating the delayed fluorescence occurred through RISC process. The phenomenon further demonstrates the efficient up-conversion from T_1 to S_1, probably attribute to the smaller ΔE_{ST}. The doped film of R-DNKP exhibited longer lifetimes relative to the neat film, which was similar to the delayed components of NKP in the neat and doped film with microsecond-scale lifetime. The temperature-dependent transient, together with small ΔE_{ST} values and high PLQY, were crucial for the TADF-based OLEDs having excellent performance. Due to the doped film displayed larger PLQY than the neat films, its delayed components with longer lifetimes were investigated.

By combining the decay times with PLQY, it obtained the various rate constants of the TADF materials in Tables 1 and S1. The fluorescence decay rate (k_F) of R-DNKP doped film was estimated to be 1.51×10^7 s^{-1}, which was larger than that neat of film (6.18×10^6 s^{-1}). Meanwhile, the intersystem crossing rates (k_{ISC}) for neat film and doped film were obtained to be 2.35×10^7 and 2.49×10^7 s^{-1}, respectively, demonstrating the emission of singlet-state exciton is almost the same as the generation of triplet-state exciton. By contrast, the RISC rate

(k_{RISC}) of 4.38 × 10^6 s^{-1} and 1.89 × 10^6 s^{-1} for neat film and doped film were relatively slower due to the process of RISC was spin-forbidden. As for NKP, the results were relatively lower than those of R-DNKP, the k_{ISC} for neat film and doped film was comparable. But the doped film of NKP displayed superior TADF property than neat film, probably resulting from a larger PLQY for DF component of doped film. Through the comparison and analysis, it was found that the larger k_{ISC} and k_{RISC} values in R-DNKP neat film were the crucial factors to shorten the lifetime of delayed fluorescence. The marked discrepancies in k_{ISC} and k_{RISC} between R-DNKP and NKP can be explained by the number of energy transition channels. Multi-channels in R-DNKP can be beneficial to accomplish a rapid conversion of excitons between singlet and triplet states.

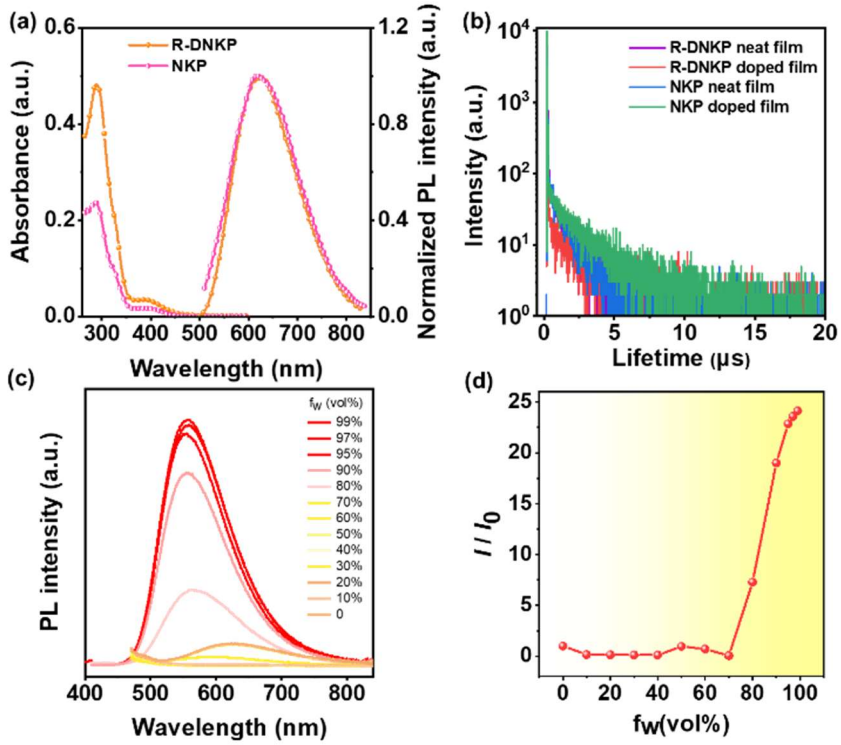

Figure 2. (a) UV-visible absorption spectra and normalized PL spectra of R-DNKP and NKP in THF (10^{-5} M). (b) Transient PL decay curves of neat film and doped film for R-DNKP and NKP. (c) The PL spectra of R-DNKP in THF/water mixtures with different water fractions (f_w, vol 0-99%). (d) Plot of emission intensity in mixtures solution/emission intensity in pure THF solution (I/I_0) versus f_w of R-DNKP.

Table 1. Photophysical properties of R-DNKP and NKP

	Neat film						Doped film[a)]					
	PLQY [%][b)]	τ_p [ns][c)]	τ_d [μs][d)]	ΔE_{ST} [eV][e)]	k_{ISC} [$10^7 s^{-1}$][f)]	k_{RISC} [$10^6 s^{-1}$][g)]	PLQY [%][b)]	τ_p [ns][c)]	τ_d [μs][d)]	ΔE_{ST} [eV][e)]	k_{ISC} [$10^7 s^{-1}$][f)]	k_{RISC} [$10^6 s^{-1}$][g)]
R-DNKP	75	31.54	0.88	0.09	2.35	4.38	94	24.41	1.35	0.07	2.49	1.89
NKP	68	22.35	1.05	0.10	1.48	1.43	88	23.60	2.08	0.08	1.95	0.89

[a)]20 wt% doped CBP film; [b)]Absolute photoluminescence quantum yield measured by integrating sphere; [c)]Transient fluorescence lifetime; [d)]Delayed fluorescence lifetime; [e)]The energy gap between S_1 and T_1 evaluated by fluorescence and phosphorescence spectrum at 77 K; [f)]The rate constant of intersystem crossing; [g)]The rate constant of reverse intersystem crossing.

2.3. Chiroptical Properties

As the axial chiral center was existed in the structure of the enantiomer, the chiroptical properties of the ground state and the excited states of R/S-DNKP were studied by CD and CPL spectroscopy, respectively. As shown in Figures 3 and S18, the CD spectra of R/S-DNKP displayed the obvious mirror-image relationship with the maximum band centered around 300 nm in neat films and solvents of different polarity (Hex, Tol and THF). The apparent Cotton effects were observed in short wavelength region at 300 and 330 nm, which can be inferred from the characteristic absorption of chiral binaphthyl moieties. It indicated that chirality was successfully induced in the ground state of the TADF group due to the chiral unit of both enantiomers. Meanwhile, the chiral enantiomers revealed good mirror-image CPL signals in films state, which further demonstrates the chiroptical properties of the luminescent molecules in the excited state. The R/S-DNKP films were prepared by spin coating, and the larger average g_{lum} values at 550 nm were measured to be $+1.1\times10^{-3}$ and -1.3×10^{-3}, respectively. These results verified that the TSC skeleton strategy based on chiral perturbation could possess the capacity to construct new chiral luminescent materials, and then obtain CPL activity with large g_{lum} value.

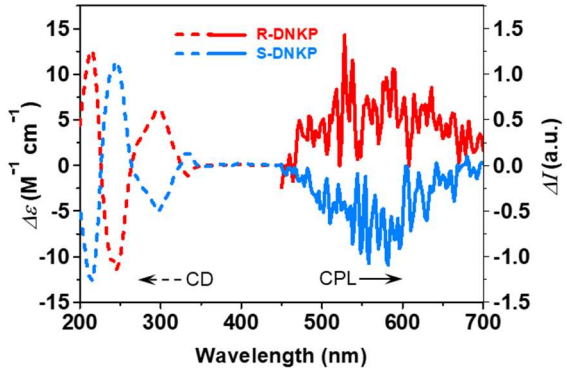

Figure 3. CD and CPL spectra of R/S-DNKP in neat films.

2.4. Theoretical Computation

The density functional theory (DFT) at the level of M06-2X/6-31G(d) was used to understand the optimized structures and energy levels. As shown in Figure 1, the geometrical optimization of R-DNKP exhibits the chiral helical folding configuration, where the two naphthalene rings are respectively parallel to the ether-linked benzene ring on benzophenone. In this case, the through-bond coupling between benzophenone and binaphthol is interrupted by ether bond. But the interplanar distances between adjacent benzene and naphthalene rings range from 2.85 to 3.46 Å, indicating that the two D-A structures may be connected by strong TSC. Moreover, the torsion angles between benzophenone and phenoxazine are about 72.6˚, which is similar to that of NKP.

From the electron cloud distribution and energy level of the highest occupied and lowest unoccupied molecular orbitals (HOMO and LUMO) in Figure 4a, the HOMO orbital is mainly localized on the phenoxazines moiety, while the LUMO is on the two benzophenone moieties and bridging binaphthol ring. This suggests that the acceptor part of R-DNKP can obtain dual-channel enhancement through TSC. The energy levels of HOMO and LUMO of R-DNKP are −4.84 eV and −1.84 eV, respectively, which is not much different from NKP. As the results of time-dependent DFT (TD-DFT) calculations, the appropriate twisted angles between donor and acceptor have achieved the small ΔE_{ST} values of 0.016 eV and 0.013 eV to activate TADF properties for R-DNKP and NKP.

The strength of homogeneous noncovalent interactions (NCIs) is conventionally estimated roughly by the distance between adjacent groups.[16] To analyze the effect of TSC on the dual-core emitter in detail, the function of reduced density gradient (RDG) and sign $(\lambda_2)\rho$ were calculated using Multiwfn program.[17] It is used for visibly analyzing the distribution and intensity of intramolecular NCIs on isosurfaces with different gradient colors.[18] As expected, the intermolecular attractive interactions (green area) between the naphthalene ring and closely face-to-face overlapped benzene ring in benzophenone in R-DNKP are presented in Figure 4b. These interactions allow the two acceptors to form an efficient excitonic coupling, which might effectively restrict the excited-state structural vibrations to suppress nonradiative pathways.

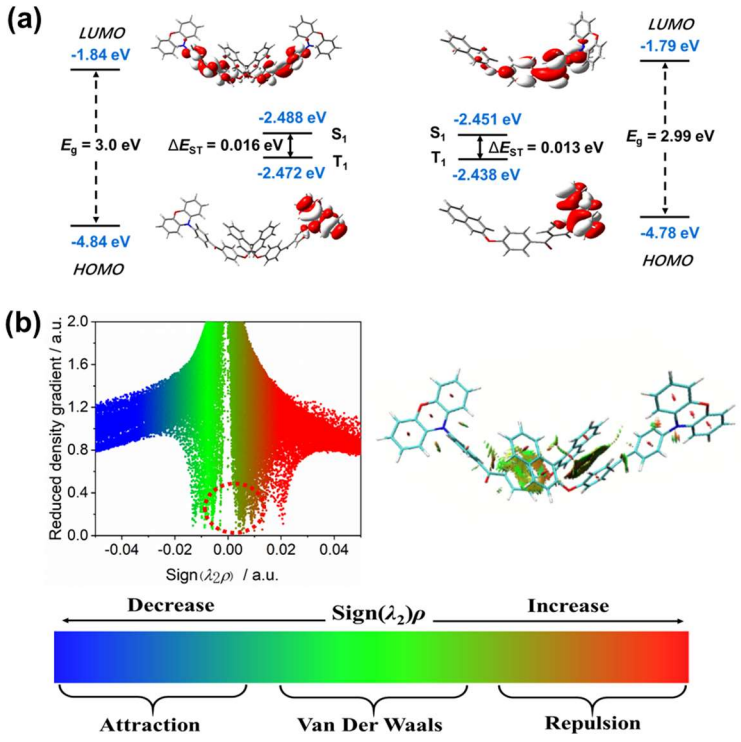

Figure 4. (a) The HOMO and LUMO orbital distributions and calculated energy levels for R-DNKP and NKP. (b) Plots of the S_{RDG} versus sign $(\lambda_2)\rho$ and the distribution of NCI regions in R-DNKP, and the isovalues of RDG are 0.5.

2.5. Electrochemical and Thermal Properties

Cyclic voltammetry (CV) was investigated to understand the electrochemical properties of these compounds in Figure S19. Base on the onset of the oxidation curve, the HOMO energy levels were calculated to be -5.14 and -5.16 eV for R-DNKP and NKP, respectively. Combined with the energy level gap (E_g), which was determined to be 2.54 eV for both compounds from the absorption edge (λ_{onset}) of the THF solution, the LUMO energy levels were found to be -2.60 and -2.62 eV for R-DNKP and NKP, respectively, ($E_{LUMO} = E_{HOMO} + E_g$). Thermal gravimetric analysis and differential scanning calorimetry were then carried out to investigate the thermal stability of the enantiomers. The dual-core emitters exhibited significantly improved thermal stability compared to their single-core counterparts. As shown in Figure S20, R-DNKP revealed very high decomposition temperatures (T_d) of 527 ˚C and a glass-transition temperature (T_g) of 144 ˚C, while the T_d value of 396 ˚C and the value of 62 ˚C for NKP. The excellent thermal stability properties are beneficial for the performance of vapor-deposited devices.

2.6. Electroluminescence Properties

Inspired by the AIE and TADF characteristics, the R/S-DNKP and NKP were respectively applied as the emitting layer in the OLEDs. The doped devices were fabricated with the configuration of indium tin oxide (ITO)/1,1'-Bis(di-4-tolylaminophenyl) cyclohexane (TAPC) (40 nm)/4,4',4"-Tris (carbazol-9-yl)-triphenylamine (TCTA) (10 nm)/20 wt% emitters: CBP (30 nm)/1,3,5-tri(m-pyrid-3-yl-phenyl) benzene (TmPyPb) (50 nm)/LiF (1 nm)/Al (100 nm), where ITO and LiF/Al are adopted as the anode and cathode, respectively; TAPC and TmPyPb functioned as hole- and electron-transporting layers, respectively; TCTA served as the exciton blocking layer; and CBP acted as the host material in the emitting layer. The energy-level

diagrams and EL characteristics of these devices are summarized in Table 2 and illustrated in Figures 5 and S21.

The devices were turned on at low turn-on voltage (V_{on}) of nearly 3.0 V, indicating efficient carrier injection and transport. And, the EL performance of the two TADF enantiomers were almost parallel. The devices of R-DNKP and S-DNKP emitted yellow EL centered at 550 nm with the maximum current efficiency (CE) of 69.38 cd A^{-1} and 63.79 cd A^{-1}, the maximum power efficiency (PE) of 68.03 lm W^{-1} and 57.93 lm W^{-1}, and the high maximum EQE of 21.5% and 19.7%, respectively. And these displayed relatively low roll-off, such as high EQE value of 19.2% and 16.7% in S-DNKP at a luminance of 1000 and 5000 cd m^{-2}, respectively. In the case of NKP-based device, a peak EQE_{max} was only 16.4%, and other EL performances were also significantly lower than those of enantiomers. The longer lifetime of NKP in doped device compared to enantiomers may lead to the decrease in EQE value. It suggests that dual-core connected by TSC can effectively reduce stronger exciton-carrier interactions and stronger electric assisted dissociation.

Furthermore, the nondoped OLEDs were investigated by similar device construction of doped devices with the difference in the emitting layer. As shown in Figure S22, the device based on R-DNKP and S-DNKP exhibited high EQE_{max} of 12.1% and 12.0% with the maximum luminance of up to 72020 cd m^{-2} and 67480 cd m^{-2}, respectively. More importantly, the devices still retained excellent EQE of 11.8% and 11.7%, respectively, at the high luminance of 5000 cd m^{-2}. The corresponding efficiency roll-off was as small as 2.5%, demonstrating the greatly advanced efficiency stability. By contrast, the EQE_{max} value of NKP was 12.4%, but the efficiency roll-off value of 6.4% at the luminance of 1000 cd m^{-2}, even up to 17.7% when the brightness reached the high brightness of 5000 cd m^{-2}. In general, if the lifetime of triplet excitons is measured in microseconds, triplet-triplet annihilation (TTA) is usually the main factor leading to the decrease of efficiency roll-off in the devices[20]. The minimal efficiency roll-off for R-DNKP-based device is primarily attributable to its nanosecond delayed lifetime

and larger k_{RISC}, which is conducive to alleviation of the triplet exciton accumulation and the suppression of the competitive exciton deactivation process under high brightness.

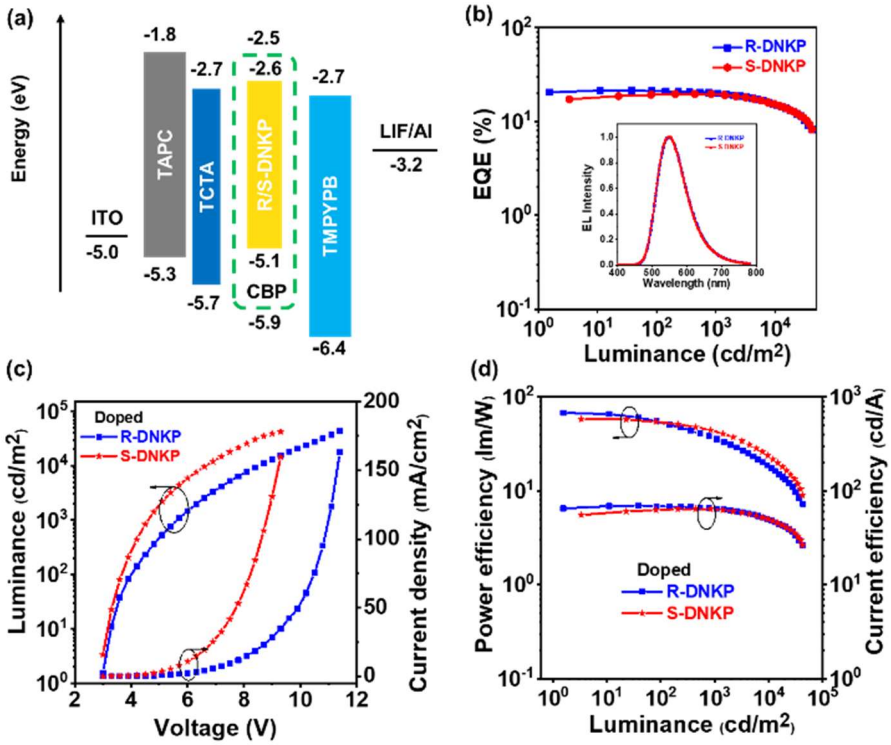

Figure 5. (a) The device structures and energy-level diagrams.(b) External quantum efficiency versus luminance plots and EL spectra (inset) of the doped devices of doped OLEDs for R/S-DNKP. (c) Current density–voltage–luminance (J–V–L) characteristics of doped OLEDs for R/S-DNKP. (d) Current density–luminance–power efficiency characteristics of doped OLEDs for R/S-DNKP.

Table 2. EL performances of the OLEDs based on R/S-DNKP and NKP.

Devices	$V_{turn-on}$ [V][a)]	λ_{EL} [nm][b)]	$CE_{max/1000/5000}$ [cd A^{-1}][c)]	$PE_{max/1000/5000}$ [lm W^{-1}][d)]	$EQE_{max/1000/5000}$ [%][e)]	Roll-off [%][f)]
R-DNKP (20 wt%)	3.0	550	69.38/64.69/55.64	68.03/35.65/23.30	21.5/20.0/17.2	7.0/20.0
S-DNKP (20 wt%)	3.0	550	63.79/62.07/54.21	57.93/40.63/228.38	19.7/19.2/16.7	2.5/15.2
NKP (20 wt%)	3.3	544	51.78/48.25/39.94	44.27/25.25/16.72	16.4/15.3/12.7	6.7/22.5
R-DNKP	2.5	564	35.82/35.82/34.90	35.13/33.10/27.41	12.1/12.1/11.8	0/2.5
S-DNKP	2.5	564	35.72/35.72/34.72	35.14/33.00/27.27	12.0/12.0/11.7	0/2.5
NKP	3.1	560	37.28/34.82/30.70	33.69/23.77/17.52	12.4/11.6/10.2	6.4/17.7

[a)]Turn-on voltage recorded at 1 cd m^{-2}; [b)]EL peak at 7 V; [c)]The maximum current efficiency and current efficiency measured at 1000 and 5000 cd m^{-2}; [d)]The maximum power efficiency and power efficiency measured at 1000 and 5000 cd m^{-2}; [e)]The maximum external quantum efficiency and external quantum efficiency measured at 1000 and 5000 cd m^{-2}; [f)]Current efficiency roll-off from the maximum value to that at 1000 or 5000 cd m^{-2}.

3. Conclusion

We demonstrated a chiral dual-core strategy for the design of chiral emitter that facilitating high EQE and little efficiency roll-off in OLEDs. The BINOL-based enantiomers R/S-DNKP were designed and synthesized by connecting two identical TADF emitters with a stable chiral unit. Compared to the mono-core counterpart NKP, the chiral dual-core emitters with TSC showed significantly increased maximum absorption coefficient, thermal stability, and excellent TADF characteristics including small ΔE_{ST} value of 0.09 and 0.07 eV, high PLQY of 75% and 94% in neat and doped films, respectively. Moreover, it achieved excellent CPL property with g_{lum} values were $+1.1\times10^{-3}$ and -1.3×10^{-3} in film states, respectively. In particular, compared with the EQE_{max} (16.4%) of NKP-based doped device, the fabricated OLEDs based on the enantiomers displayed a significantly enhanced EQE_{max} of 21.5% and 19.7% with yellow light emission at around 550 nm. Besides, the device features an EQE of 20.0% and 19.2% at 1000 cd m^{-2} with remarkably low efficiency roll-off of 7.0% and 2.5%. Due to the combination of AIE and TADF characteristics, the non-doped devices fabricated by the enantiomers also possessed superior EL efficiencies with extremely small roll-off (2.5%) at high luminance of 5000 cd m^{-2}, which was also the one of the best reported so far using the dual-core by TSC strategy. Thus, we believe that the combination of chiral fragment (such as axial, planar, helical or propeller chirality) and TADF skeleton using TSC provides a feasible idea to design high-performance OLEDs.

Acknowledgements

This work was supported by the National Natural Science Foundation of China (No. 52273168, U2001222, 21975055, 92256202, 22221001 and 51733004), State Key Laboratory of Optoelectronic Materials and Technologies (OEMT-2022-KF-01) and Guangdong Province Universities and Colleges Pearl River Scholar Funded Scheme (2019) for financial support.

Conflict of Interests

The authors declare no conflict of interests.

Supporting Information

Supporting Information is available from the Wiley Online Library or from the author.

Received: ((will be filled in by the editorial staff))
Revised: ((will be filled in by the editorial staff))
Published online: ((will be filled in by the editorial staff))

References

1. a) Y. Tao, K. Yuan, T. Chen, P. Xu, H. Li, R. Chen, C. Zheng, L. Zhang, W. Huang, *Adv. Mater.* **2014**, *26*, 7931; b) Y. Liu, C. Li, Z. Ren, S. Yan, M. R. Bryce, *Nat. Rev. Mater.* **2018**, *3*, 18020; c) Q. Li, Y. Tang, W. Hu, Z. Li, *Small* **2018**, *14*, 1801560.

2. a) D. Ding, Z. Wang, C. Li, J. Zhang, C. Duan, Y. Wei, H. Xu, *Adv. Mater.* **2020**, *32*, 1906950; b) J. Zhang, Q. Wei, N. Fei, M. Zhao, L. Xie, L. Cao, X. Zhang, G. Xie, T. Wang, Z. Ge, *ACS Appl. Mater. Interfaces* **2021**, *13*, 12305.

3. a) C. Murawski, K. Leo, M. C. Gather, *Adv. Mater.* **2013**, *25*, 6801; b) L. Zhou, L. Yang, M. Yu, Y. Jiang, C.-F. Liu, W.-Y. Lai, W. Huang, *ACS Appl. Mater. Interfaces* **2017**, *9*, 40533; c) H. Chen, J. Zeng, R. Huang, J. Wang, J. He, H. Liu, D. Yang, D. Ma, Z. Zhao, B. Z. Tang, *Aggregate* **2023**, *4*, e244.

4. a) S. Xu, T. Liu, Y. Mu, Y. F. Wang, Z. Chi, C. C. Lo, S. Liu, Y. Zhang, A. Lien, J. Xu, *Angew. Chem. Int. Ed.* **2015**, *54*, 874; b) Z. Huang, Z. Bin, R. Su, F. Yang, J. Lan, J. You, *Angew. Chem. Int. Ed.* **2020**, *59*, 9992.

5. a) S. Ullbrich, J. Benduhn, X. Jia, V. C. Nikolis, K. Tvingstedt, F. Piersimoni, S. Roland, Y. Liu, J. Wu, A. Fischer, D. Neher, S. Reineke, D. Spoltore, K. Vandewal, *Nat. Mater.* **2019**, *18*, 459; b) X.-Q. Wang, S.-Y. Yang, Q.-S. Tian, C. Zhong, Y.-K. Qu, Y.-J. Yu, Z.-Q. Jiang, L.-S. Liao, *Angew. Chem. Int. Ed.* **2021**, *60*, 5213; c) Y. Fu, Z. Ye, D. Liu, Y. Mu, J. Xiao, D. Hu, S. Ji, Y. Huo, S. J. Su, *Adv. Mater.* **2023**, *35*, 2301929.

6. a) J. Huang, H. Nie, J. Zeng, Z. Zhuang, S. Gan, Y. Cai, J. Guo, S. J. Su, Z. Zhao, B. Z. Tang, *Angew. Chem. Int. Ed.* **2017**, *56*, 12971; b) I. S. Park, K. Matsuo, N. Aizawa, T. Yasuda, *Adv. Funct. Mater.* **2018**, *28*, 1802031; c) J.-X. Chen, Y.-F. Xiao, K. Wang, D. Sun, X.-C. Fan, X.

Zhang, M. Zhang, Y.-Z. Shi, J. Yu, F.-X. Geng, C.-S. Lee, X.-H. Zhang, *Angew. Chem. Int. Ed.* **2021**, *60*, 2478.

7. a) G. Méhes, H. Nomura, Q. Zhang, T. Nakagawa, C. Adachi, *Angew. Chem. Int. Ed.* **2012**, *51*, 11311; b) Y. Mu, B. Xu, Z. Yang, H. Wen, Z. Yang, S. K. B. Mane, J. Zhao, Y. Zhang, Z. Chi, B. Z. Tang, *ACS Appl. Mater. Interfaces* **2020**, *12*, 5073.

8. a) S. Xu, Y. Duan, P. Manghnani, Kenry, C. Chen, S. M. Kozlov, B. Liu, *Adv. Mater.* **2021**, *33*, 2100986; b) S. Xu, J. Li, P. Cai, X. Liu, B. Liu, X. Wang, *J. Am. Chem. Soc.* **2021**, *143*, 19769.

9. a) Y. J. Cho, S. K. Jeon, B. D. Chin, E. Yu, J. Y. Lee, *Angew. Chem. Int. Ed.* **2015**, *54*, 5201; b) D. Wei, F. Ni, Z. Wu, Z. Zhu, Y. Zou, K. Zheng, Z. Chen, D. Ma, C. Yang, *J. Mater. Chem. C* **2018**, *6*, 11615; c) Y.-F. Wang, M. Li, W.-L. Zhao, Y.-F. Shen, H.-Y. Lu, C.-F. Chen, *Chem. Commun.* **2020**, *56*, 9380; d) Z.-P. Yan, L. Yuan, Y. Zhang, M.-X. Mao, X.-J. Liao, H.-X. Ni, Z.-H. Wang, Z. An, Y.-X. Zheng, J.-L. Zuo, *Adv. Mater.* **2022**, *34*, 2204253.

10. a) S. Feuillastre, M. Pauton, L. Gao, A. Desmarchelier, A. J. Riives, D. Prim, D. Tondelier, B. Geffroy, G. Muller, G. Clavier, G. Pieters, *J. Am. Chem. Soc.* **2016**, *138*, 3990; b) S. Sun, J. Wang, L. Chen, R. Chen, J. Jin, C. Chen, S. Chen, G. Xie, C. Zheng, W. Huang, *J. Mater. Chem. C* **2019**, *7*, 14511; c) S.-Y. Yang, Y.-K. Wang, C.-C. Peng, Z.-G. Wu, S. Yuan, Y.-J. Yu, H. Li, T.-T. Wang, H.-C. Li, Y.-X. Zheng, Z.-Q. Jiang, L.-S. Liao, *J. Am. Chem. Soc.* **2020**, *142*, 17756; d) M. Li, M.-Y. Wang, Y.-F. Wang, L. Feng, C.-F. Chen, *Angew. Chem. Int. Ed.* **2021**, *60*, 20728.

11. a) F. Song, Z. Xu, Q. Zhang, Z. Zhao, H. Zhang, W. Zhao, Z. Qiu, C. Qi, H. Zhang, H. H. Y. Sung, I. D. Williams, J. W. Y. Lam, Z. Zhao, A. Qin, D. Ma, B. Z. Tang, *Adv. Funct. Mater.* **2018**, *28*, 1800051; b) L. Zhou, F. Ni, N. Li, K. Wang, G. Xie, C. Yang, *Angew. Chem. Int. Ed.* **2022**, *61*, e202203844.

12. a) J. Li, P. Shen, Z. Zhao, Z. Tang Ben, *CCS Chem.* **2019**, *1*, 181; b) C. Hua, P. W. Doheny, B. Ding, B. Chan, M. Yu, C. J. Kepert, D. M. D'Alessandro, *J. Am. Chem. Soc.* **2018**, *140*, 6622; c) S. Xu, B. Liu, *J. Am. Chem. Soc.* **2022**, *144*, 17897.

13. a) L. Chen, Y.-H. Wang, B. He, H. Nie, R. Hu, F. Huang, A. Qin, X.-S. Zhou, Z. Zhao, B. Z. Tang, *Angew. Chem. Int. Ed.* **2015**, *54*, 4231; b) S. Zhen, J.-C. Mao, L. Chen, S. Ding, W. Luo, X.-S. Zhou, A. Qin, Z. Zhao, B. Z. Tang, *Nano Lett.* **2018**, *18*, 4200.

14. a) E. Spuling, N. Sharma, I. D. W. Samuel, E. Zysman-Colman, S. Bräse, *Chem. Commun.* **2018**, *54*, 9278; b) C. Liao, Y. Zhang, S.-H. Ye, W.-H. Zheng, *ACS Appl. Mater. Interfaces* **2021**, *13*, 25186; c) P. Shen, H. Liu, Z. Zhuang, J. Zeng, Z. Zhao, B. Z. Tang, *Adv. Sci.* **2022**,

9, 2200374; d) Y.-P. Zhang, M.-X. Mao, S.-Q. Song, Y. Wang, Y.-X. Zheng, J.-L. Zuo, Y. Pan, *Angew. Chem. Int. Ed.* **2022**, *61*, e202200290.

15. a) S. Yu, L. Pu, *Tetrahedron* **2015**, *71*, 745; b) Y. Sang, J. Han, T. Zhao, P. Duan, M. Liu, *Adv. Mater.* **2020**, *32*, 1900110; c) D.-W. Zhang, M. Li, C.-F. Chen, *Chem. Soc. Rev.* **2020**, *49*, 1331; d) Y. Zhang, S. Yu, B. Han, Y. Zhou, X. Zhang, X. Gao, Z. Tang, *Matter* **2022**, *5*, 837.

16. a) J. Guo, X.-L. Li, H. Nie, W. Luo, R. Hu, A. Qin, Z. Zhao, S.-J. Su, B. Z. Tang, *Chem. Mater.* **2017**, *29*, 3623; b) Z. Qiu, W. Xie, Z. Yang, J.-H. Tan, Z. Yuan, L. Xing, S. Ji, W.-C. Chen, Y. Huo, S.-J. Su, *Chem. Eng. J.* **2021**, *415*, 128949; c) H. J. Kim, S. K. Kim, M. Godumala, J. Yoon, C. Y. Kim, J.-E. Jeong, H. Y. Woo, J. H. Kwon, M. J. Cho, D. H. Choi, *Chem. Commun.* **2019**, *55*, 9475; d) G. Yang, Y. Ran, Y. Wu, M. Chen, Z. Bin, J. You, *Aggregate* **2022**, *3*, e127.

17. Z. Yang, E. Ubba, Q. Huang, Z. Mao, W. Li, J. Chen, J. Zhao, Y. Zhang, Z. Chi, *J. Mater. Chem. C* **2020**, *8*, 7384.

18. a) T. Lu, F. Chen, *J. Comput. Chem.* **2012**, *33*, 580; b) L. Chen, J.-H. Tan, Z. Yang, Z. Qiu, Y. Mu, Z. Yang, W.-C. Chen, S. Ji, Z. Chi, Y. Huo, *J. Lumin.* **2021**, *230*, 117731.

19. E. R. Johnson, S. Keinan, P. Mori-Sánchez, J. Contreras-García, A. J. Cohen, W. Yang, *J. Am. Chem. Soc.* **2010**, *132*, 6498.

20. a) J. Lee, N. Aizawa, T. Yasuda, *Chem. Mater.* **2017**, *29*, 8012; b) B. Li, Z. Wang, S.-J. Su, F. Guo, Y. Cao, Y. Zhang, *Adv. Opt. Mater.* **2019**, *7*, 1801496.

The chiral BINOL group could be used to link two thermally activated delayed fluorescence molecules to obtain dual-core enantiomers. Owning to efficient through-space coupling, the photoluminescence and electroluminescence properties are significantly improved compared with the mono-core counterpart.

aggregation-induced emission, thermally activated delayed fluorescence, through-space coupling, circularly polarized luminescence, organic light-emitting diodes

L. Chen, M. Deng, S.-Y. Yin, Y. Fu, Y. Mu,* J.-X. Chen, L. Cui,* S. Ji, Y. Huo* and H.-L. Zhang*

Chiral dual-core AIEgens based-on through-space coupling for high-performance organic light-emitting diodes with little efficiency roll-off